IEEE Access
Multidisciplinary | Rapid Review | Open Access Journal

Received 5 February 2024, accepted 20 February 2024, date of publication 26 February 2024, date of current version 5 March 2024.

Digital Object Identifier 10.1109/ACCESS.2024.3370561

RESEARCH ARTICLE

Radar Cardiogram Extraction and Respiratory Harmonic Suppression Based on Optimized Feedback Notch Filters

YARU WANG[1,2], JIAHAO QIAO[1,2], KEDING YAN[1], DING SHI[1,2], YIDAN ZHU[1,2], XINYU WANG[1,2], HUIJUN XUE[2], FULAI LIANG[2], XIAO YU[2], TENG JIAO[2], HAO LV[2], JIANQI WANG[2], WENZONG LU[1], AND YANG ZHANG[2]

[1]School of Electronic and Information Engineering, Xi'an Technological University, Xi'an 710021, China
[2]Department of Medical Electronics, School of Biomedical Engineering, Shaanxi Provincial Key Laboratory of Bioelectromagnetic Detection and Intelligent Perception, Air Force Medical University, Xi'an 710032, China

Corresponding authors: Wenzong Lu (luwenzong@xatu.edu.cn) and Yang Zhang (yangzhang@fmmu.edu.cn)

This work was supported in part by the Air Force Medical University Talent Program under Grant 2022-fhjsyxrc19, in part by the Basic Research Project of Natural Sciences of Shaanxi Province under Grant 2020JM-559, and in part by the National Natural Science Foundation of China under Grant 62371454.

This work involved human subjects or animals in its research. Approval of all ethical and experimental procedures and protocols was granted by the Ethic Committee of the Affiliated Hospital of Air Force Medical University.

ABSTRACT Radar is a valuable tool for noncontact vital-sign detection. Interference from respiratory harmonics presents a major challenge in radar cardiogram (RCG) extraction—mainly when the frequency of respiratory harmonics is close to or equal to that of the cardiac sub-signals. To address this problem, a respiratory harmonic suppression method employing correlation analysis and an optimized feedback notch filter is proposed, which is based on 7.29 GHz center-frequency impulse-radio ultra-wideband radar. A genetic optimization algorithm is employed to optimize the parameters of the notch filter. Performance comparison analysis is conducted on the conventional notch filter and the feedback notch filter. Contact (ECG) and non-contact (RCG) data from 10 subjects were analyzed. The results verified that the performance of the optimized feedback notch filter is much better than that of the conventional notch filter in overshoot, bandwidth, and notch depth, and the proposed method can effectively locate, identify, and suppress respiratory harmonics from the RCG band while preserving heartbeat components. Consequently, this approach markedly enhances the precision of RCG extraction. The technique shows considerable promise for deployment in diverse practical settings, including non-contact auxiliary monitoring systems in both intelligent medical environments and home healthcare.

INDEX TERMS Correlation analysis, feedback notch filter, genetic algorithm, radar cardiogram, respiratory harmonic suppression.

I. INTRODUCTION

Cardiopulmonary signals, i.e., cardiograms and respiratory signals, are crucial physiological parameters for clinical diagnosis and disease prevention [1], [2]. Commercial cardiogram measurement methods include electrocardiography (ECG), phonocardiography, ballistocardiography, and photoplethysmography, all of which are based on contact-probe attachment and thus have limited applications. In comparison, contactless measurement technologies such as bio-radar have significant advantages for the clinical monitoring of burn injuries, infectious diseases, sudden infant death syndrome, etc. [3], [4], [5]. Bio-radar detects vital signs by measuring subtle chest movements caused by heartbeats and respiration. It can be largely divided into continuous-wave (CW) radar and ultra-wideband (UWB) radar. Owing to

The associate editor coordinating the review of this manuscript and approving it for publication was Tianhua Xu.

its advantages of a high distance resolution, low power consumption [6], [7], and powerful penetration compared with CW radar, impulse-radio ultra-wideband (IR-UWB) radar is attracting increasing attention for human vital-sign detection [8], [9].

The extraction of cardiac signals presents two challenges. First, the chest displacement variation caused by cardiac motion is significantly smaller than that caused by respiration, which makes the extraction of cardiac signals difficult. Second, the presence of respiratory harmonics interferes substantially with cardiac signals. Researchers have attempted to extract subtle cardiac signals from respiratory signals via radar detection [10] and have used bandpass and adaptive filters to extract heartbeat signal waveforms. Additionally, a variational modal decomposition algorithm has been used to estimate heartbeat signals [11], [12]. In [13], an adaptive recursive least-squares method was used to separate respiratory and heartbeat signals. In [14], the heart rate was accurately determined using a combination of empirical modal decomposition and principal component analysis. However, radar signals contain several respiratory harmonics [15], [16], [17] which lead to radar cardiac signal distortion and inaccurate heart rate estimation, significantly interfering with the extraction of the cardiac signal. Some of these harmonics are close to or even completely overlap with the radar cardiac signal in the frequency domain; thus, the challenge is difficult to retain the cardiac signal through the precise suppression of respiratory harmonics. To address this problem, a parametric respiratory filter was proposed [18] for precisely suppressing respiratory harmonics; however, the situation of overlapping respiratory harmonics and cardiac signals was not considered.

In this paper, a method using correlation analysis is proposed for determining whether the respiratory harmonic coincides with the radar cardiogram (RCG) at each respiratory harmonic frequency point. If so, the signal at this frequency is considered as a heartbeat component and is retained. Otherwise, it is considered as a respiratory harmonic and must be suppressed. A parameter-optimization feedback notch filter based on a genetic algorithm was designed for respiratory harmonic suppression. The optimized filter has an extremely narrow bandwidth and the best notch performance, which guarantee minimal loss of heartbeat components during harmonic suppression. Simulation and experimental results indicated that the proposed method can accurately remove respiratory harmonics while retaining the detailed information of the radar cardiac signal well.

II. METHODS

An IR-UWB radar with a center frequency of 7.29 GHz was applied to acquire vital-sign signals. The radar echo data were processed as follows. First, preprocessing was adopted [19] to remove static clutter and high-frequency noise. Second, the respiratory signal and radar cardiogram (RCG) were separated from the preprocessed signal using filters of different bands. Then, the respiratory harmonic signals were generated via multiplication and frequency interpolation from the respiratory signal. At the same time, localization of respiratory harmonics in the RCG was executed. Finally, respiratory harmonic suppression was performed after determining whether there was an overlap. A flowchart of the cardiogram extraction and respiratory harmonic suppression is presented in Figure 1.

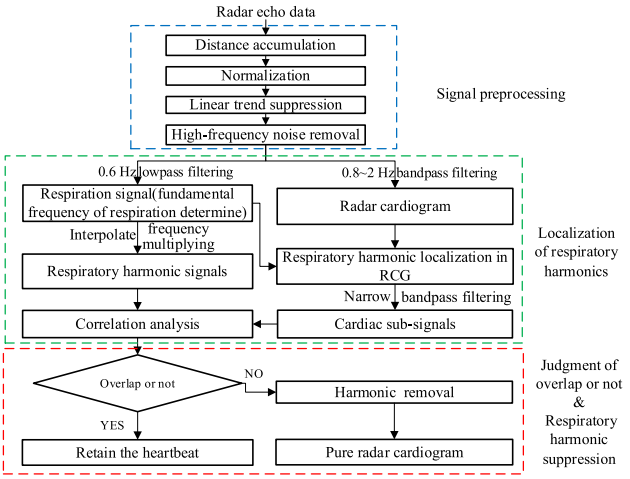

FIGURE 1. Flowchart of cardiogram extraction and respiratory harmonic suppression.

A. SIGNAL PREPROCESSING

The signal preprocessing steps include distance (fast-time dimension) accumulation, normalization, linear trend suppression (LTS), and high-frequency noise removal.

1) DISTANCE ACCUMULATION

The received radar echo data are stored in a two-dimensional matrix $R(m, n)$, m represents the propagation time, which is called the fast-time dimension which can be converted into range dimension, and the unit is nanoseconds or meters; n denotes the observation time, which is called slow-time dimension, and is measured in seconds. Because the modulation of radar echoes at neighboring distance points in the fast-time dimension is approximately the same, distance accumulation of the radar echo data $R(m, n)$ in the fast-time dimension is first performed to reduce the computational cost without losing useful information.

$$R_1(l, n) = \frac{1}{Q} \sum_{m=Q(l-1)+1}^{Ql} R(m, n) \tag{1}$$

Here, $R_1(l, n)$ $(l = 1, 2, 3, \ldots, L)$ represents the distance-accumulated echo data, Q represents the accumulated window width in the fast time dimension, and L represents the number of distance points in the fast time dimension after accumulation; $L = \lfloor M/Q \rfloor$, with "$\lfloor\ \rfloor$" denoting rounding down. Distance accumulation can significantly reduce the computational cost of subsequent radar data processing. To some extent, distance accumulation is equivalent to

smooth filtering, which can suppress high-frequency interference in the fast-time dimension.

2) NORMALIZATION

Considering the propagation attenuation of radar signals, to compensate the amplitude of the target signal at a longer distance from the radar and increase the signal-to-noise ratio (SNR) of the signal, the signal $R_1(l, n)$ normalized in the slow-time dimension is expressed as

$$R_2(l,n) = 2 \times \frac{R_1(l,n) - \min\limits_{0\le n\le N}[R_1(l,n)]}{\max\limits_{0\le n\le N}[R_1(l,n)] - \min\limits_{0\le n\le N}[R_1(l,n)]} - 1 \tag{2}$$

where $R_2(l, n)$ represents the normalized data, and N represents the number of slow-time signal points contained in the data. After normalization, the amplitude of the slow-time signal at each distance ranges from –1 to 1.

3) LINEAR TREND SUPPRESSION

During real data acquisition, static background clutter and drift of the echo baseline are inevitable and affect the extraction of subtle human signals [20]. Therefore, LTS was used to remove static clutter and linear drift after normalization.

$$R_3(l,n) = R_2(l,n) - \frac{1}{N}\sum\nolimits_N^1 R_2(l,n) \tag{3}$$

Here, $R_3(l, n)$ represents the data after linear drift elimination and static clutter removal.

4) HIGH-FREQUENCY NOISE REMOVAL

Because radar hardware generates high-frequency noise during its operation and the human cardiac or respiratory signal is a narrow-band quasi-periodic signal, low-pass filtering in the slow-time dimension is applied to remove the high-frequency noise and further improve the SNR of the radar signal.

$$R_4(l,n) = R_3(l,n) * h(t) \tag{4}$$

Here, $R_4(l, n)$ represents the filtered data, "$*$" denotes the convolution operation, $h(t)$ is the impulse function of the finite impulse response low-pass filter, and the cutoff frequency of the filter is 2.5 Hz according to the range of the human cardiopulmonary movement frequency.

Radar echo data obtained before and after preprocessing are shown in Figure 2. After Signal preprocessing of noise and clutter interference removal and vital-sign extraction, a clear signal is obtained, making it easier to observe the true respiration and RCG of the target who is approximately 0.8m away from the UWB radar under free-space condition.

B. LOCALIZATI ON OF RESPIRATORY HARMONICS

According to the normal human heart rate and respiratory rate of approximately 48–120 beats per minute and 6–36 beats per minute, respectively [21], a bandpass filter (0.8–2 Hz) and a low-pass filter (∼0.6 Hz) were used to extract the radar cardiogram and the respiration signal.

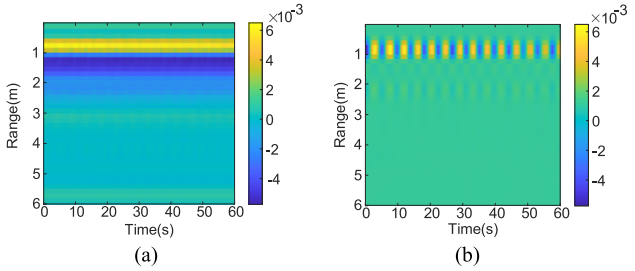

FIGURE 2. Radar echo data obtained (a) before and (b) after preprocessing.

Following the extraction of the respiration signal, the fundamental frequency of respiration was determined via fast Fourier transform of the respiration signal. Then, the frequency of each respiratory harmonic was calculated using the fundamental frequency of respiration. Equations (5) and (6) describe the localization of the respiratory harmonic frequencies.

$$R_{bx}, R_{by} = \text{maxvalue}[F\left(R_{Lp}\right)] \tag{5}$$

$$R_b = kR_{bx} \tag{6}$$

Here, maxvalue is the maximum solution function, $F(R_{LP})$ represents the respiration signal in the frequency domain, R_{bx} represents the fundamental frequency of respiration, R_{by} represents the corresponding amplitude, R_b represents the k^{th} respiratory harmonic frequency, and k represents the ordinal number of harmonics.

As we know, the respiratory harmonic frequency is an integer multiple of the fundamental frequency of respiration. Generally, the 3rd, 4th, and 5th human respiratory harmonics fall within the RCG band. Thus, after the fundamental frequency of respiration and the respiratory harmonic frequencies were determined, the respiration signal was interpolated into three, four, and five frequency-multiplying signals via spline interpolation. These frequency-multiplying signals were considered as respiratory harmonic signals.

Additionally, a bandpass filter was applied to separate the RCG, which was mixed with the respiratory harmonic interference. After the respiratory harmonic frequency localization in the RCG, a series of cardiac sub-signals were extracted from RCG via a series of narrow bandpass filters with the passband center frequency located at each respiratory harmonic's frequency.

C. CORRELATION ANALYSIS

After localization of respiratory harmonics, a correlation analysis was performed to determine whether there was a frequency overlap between respiratory harmonic signals and cardiac sub-signals. If there was an overlap, the signal at the coincident frequency point was retained as the heartbeat component; otherwise, a parameter-optimized feedback notch filter was used to remove the respiratory harmonic. The correlation analysis for each respiratory harmonic signal and the corresponding cardiac sub-signal is presented below.

In [22], the number of human targets during radar localization was determined by calculating the Pearson correlation coefficients of the signals from different radar channels. In the present study, the Pearson correlation coefficient $C_{pearson}$ was calculated to determine whether the frequency of the respiratory harmonics coincided with the corresponding cardiac sub-signal.

$$C_{pearson} = \frac{\sum_{i=1}^{n}\left(R_{hi}-\overline{R_h}\right)\left(R_{fi}-\overline{R_f}\right)}{\sqrt{\sum_{i=1}^{n}\left(R_{hi}-\overline{R_h}\right)^2}\sqrt{\sum_{i=1}^{n}\left(R_{fi}-\overline{R_f}\right)^2}} \tag{7}$$

Here, n represents the length of the signal, R_{hi} represents the value of the cardiac sub-signal, $\bar{R}_h$ represents the average value of the cardiac sub-signal, R_{fi} represents the value of the respiratory harmonic signal, and $\bar{R}_f$ represents the average value of the respiratory harmonic signal.

A threshold K is set to identify the coincidence. When the calculation result $C_{pearson}$ exceeds K, it indicates that there is a high correlation and similarity between the cardiac sub-signal and the respiratory harmonic, the cardiac sub-signal is regarded as a pure harmonic interference and is removed. Otherwise, it means that the cardiac sub-signal has other frequency components in addition to the harmonic component. So, it is regarded as heartbeat component signal only coinciding with the respiratory harmonic and thus is retained.

We analyzed a large amount of real human data to derive each correlation coefficient for the overlapping data pairs and calculated the average value of all these correlation coefficients K_1. Additionally, the average value of the correlation coefficient K_2 for all non-overlapping data pairs was calculated. In this process, contact measurements using the respiratory straps and ECG equipment were performed synchronously to check whether there was a coincidence as a label. Subsequently, the threshold was determined as $K = K_2 + \frac{K_1-K_2}{2}$.

D. OVERVIEW AND PERFORMANCE ANALYSIS OF FEEDBACK NOTCH FILTER

The conventional notch filter (without feedback structure) is a special type of band-stop filter with a narrow stopband that blocks the signal at a certain frequency. The transfer function is given by Equation (8).

$$G_n(z) = \frac{1 - 2\cos(\omega')z^{-1} + z^{-2}}{1 - 2\rho\cos(\omega')z^{-1} + \rho^2 z^{-2}} \tag{8}$$

Here, ω' represents the center frequency of the stopband, i.e., the notch frequency, and ρ represents the pole radius of the transfer function $G_n(z)$. The transfer function is stable when ρ is in the range of 0–1. The performance of the notch filter is described by three parameters: the overshoot, bandwidth, and notch depth. The filter must have the minimum bandwidth, maximum attenuation at the notch frequency, and minimum overshoot to achieve optimal performance.

The amplitude-frequency characteristic curves of the notch transfer function $G_n(z)$ corresponding to different ρ values are shown in Figure 3. The bandwidth and overshoot of the notch decrease as ρ increases, but the bandwidth of the notch and the overshoot are still too large to achieve the optimal trapping performance. If it is applied directly to the removal of respiratory harmonics, a large amount of the cardiac detail information will be lost.

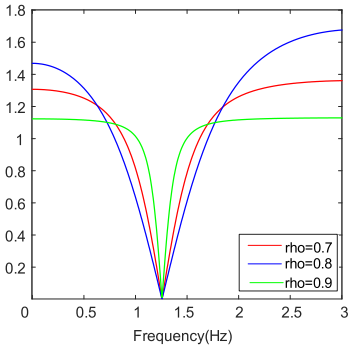

FIGURE 3. Amplitude-frequency characteristic curves of conventional notch filters with different pole radii ρ (notch frequency is 1.25 Hz).

The feedback structure was applied to create a feedback notch filter, and the corresponding transfer function is given by Equation (9).

$$Y_N(z) = \frac{(1+\alpha)G_n(Z)}{1+\alpha G_n(Z)} \tag{9}$$

Here, α is the feedback coefficient, and the notch filter is stable when $\alpha \geq 0$. The feedback notch filter degenerates to an open-loop filter at $\alpha = 0$. A block diagram of the feedback notch filter is presented in Figure 4(a). To compare the performance of the feedback notch filter, the amplitude-frequency characteristic curves of the notch transfer function $Y_N(z)$ were obtained by changing the feedback coefficient α while fixing $\rho = 0.5$ in $G_n(z)$, as shown in Figure 4(b). A comparison of the blue, green, and red lines reveals that a larger value of α corresponds to a smaller overshoot and bandwidth. The feedback structure can significantly improve the notch performance as α increases.

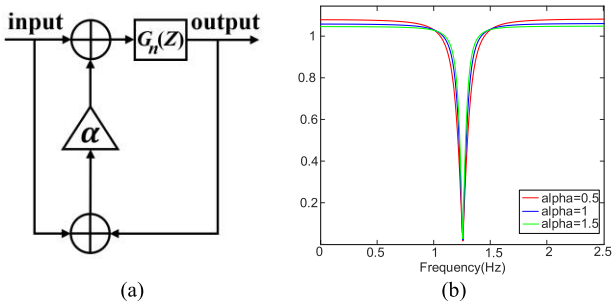

FIGURE 4. Feedback notch filter: (a) block diagram; (b) amplitude-frequency characteristic curves with different feedback coefficients α (notch frequency is 1.25 Hz).

To better illustrate the improvement of the feedback structure, the performance of the feedback notch filter and the conventional notch filter are compared.

In order to transform the complex signals from the complex frequency domain to the frequency domain. The Z variables in $G_n(z)$ are replaced with angular frequency ω, followed by the differentiation of $Y_N(\omega)$:

$$\begin{aligned} \boldsymbol{Y}_N^{'}(\boldsymbol{\omega}) &= \frac{(1+\alpha)}{[1+\alpha \boldsymbol{G_n}(\boldsymbol{\omega})]^2} \boldsymbol{G_n}'(\boldsymbol{\omega}) \\ &\Rightarrow \boldsymbol{Y_N}'(\boldsymbol{\omega}_0) = (1+\alpha)\,\boldsymbol{G_n}'(\omega_0) \\ &\Rightarrow \left|\boldsymbol{Y_N}'(\boldsymbol{\omega_0})\right| = (1+\alpha)\left|\boldsymbol{G_n}'(\boldsymbol{\omega_0})\right| \end{aligned} \tag{10}$$

Here, $G_n'(\omega)$ is a first-order differentiator of $G_n(\omega)$, ω_0 represents the notch frequency, and $\omega = \omega_0$, $G_n(\omega_0)$, and $Y_n(\omega_0)$ are equal to 0 according to the characteristics of the notch filter.

Thus, when $\alpha \neq 0$ and $\alpha > 0$,

$$|\boldsymbol{Y_N}'(\boldsymbol{\omega_0})| > |\boldsymbol{G_n}'(\boldsymbol{\omega_0})| \tag{11}$$

From the above, it is evident that the rate of decrease in the feedback structure notch filter $Y_N(\omega)$ is better than that of the unimproved notch filter $G_n(\omega)$.

The feedback structure also improves the performance of the notch filter by reducing the bandwidth. The point where the amplitude of the amplitude-frequency characteristic curve declines to $1/\sqrt{2}$ of the maximum amplitude, i.e., the -3 dB frequency point, is called the half-power point of the notch filter. There are two -3 dB frequency points symmetrically distributed on the two sides of the central notch frequency $\omega = \omega_0$ in the filter. For a better comparison, we defined $\omega_{-3\text{dB}}$ as the right half-power point of the feedback structure notch filter and $\omega^*_{-3\text{dB}}$ as the right half-power point of the conventional notch filter. The bandwidths of the two types of notch filters are given as follows:

$$\begin{aligned} &\text{bw}_1 = 2(\omega_{-3\text{dB}} - \omega_0),\ \text{bw}_2 = 2(\omega^*_{-3\text{dB}} - \omega_0) \\ &|\boldsymbol{Y_N}(\boldsymbol{\omega}_{-3\boldsymbol{dB}})| = \frac{\mathbf{1}}{\sqrt{\mathbf{2}}} \\ &|\boldsymbol{G_n}(\boldsymbol{\omega}^*_{-3\boldsymbol{dB}})| = \frac{\mathbf{1}}{\sqrt{\mathbf{2}}} \end{aligned} \tag{12}$$

$$\begin{aligned} \Rightarrow |\boldsymbol{Y_N}(\boldsymbol{\omega}_{-3\boldsymbol{dB}})| &= \frac{|(1+\alpha)\boldsymbol{G_n}(\boldsymbol{\omega}_{-3\boldsymbol{dB}})|}{|1+\alpha \boldsymbol{G_n}(\boldsymbol{\omega}_{-3\boldsymbol{dB}})|} \\ &= \frac{\mathbf{1}}{\sqrt{\mathbf{2}}} \end{aligned} \tag{13}$$

When $\alpha > 0$,

$$|\boldsymbol{G_n}(\boldsymbol{\omega}_{-3\boldsymbol{dB}})| = \frac{\mathbf{1}}{\sqrt{\mathbf{2}} + (\sqrt{\mathbf{2}} - \mathbf{1})\boldsymbol{\alpha}} \leq \frac{\mathbf{1}}{\sqrt{\mathbf{2}}} \tag{14}$$

Thus, the following formula can be obtained:

$$|\boldsymbol{G_n}(\boldsymbol{\omega}_{-3\boldsymbol{dB}}\ )| \leq \frac{\mathbf{1}}{\sqrt{\mathbf{2}}} = |\boldsymbol{G_n}(\boldsymbol{\omega}^*_{-3\boldsymbol{dB}})| \tag{15}$$

The relationship between the frequencies of the two types of notch filters with and without a feedback structure at the half-power point is $\omega_{-3\text{dB}} < \omega^*_{-3\text{dB}}$. Thus, $\text{bw}_1 < \text{bw}_2$.

From the above comparison, the rate of decrease and bandwidth of the feedback structure notch filter are superior to those of the conventional notch filter.

To better evaluate the filtering performance of the feedback notch filters, the sum of the overshoot, bandwidth, and reciprocal of the notch depth was calculated. A smaller value of the sum parameter often indicates better performance.

The results for different ρ values obtained with a fixed notch frequency of 1.5 Hz and feedback coefficient of $\alpha = 0.8$ are presented in Table 1. The results for different α values obtained with a fixed notch frequency of 1.5 Hz and pole radius of $\rho = 0.5$ are presented in Table 2.

TABLE 1. Sum parameters with different pole radii ($\alpha = 0.8$).

ρ	Sum parameter
0.1	2.59
0.2	2.78
0.3	2.60
0.4	2.44
0.5	2.32
0.6	2.19
0.7	2.06
0.8	1.89
0.9	1.68

TABLE 2. Sum parameters with different feedback coefficients ($\rho = 0.5$).

α	Sum parameter
0.2	1.81
0.4	1.83
0.6	1.78
0.8	1.77
1.0	1.79
1.2	1.74
1.4	1.73
1.6	1.77
1.8	1.76

As indicated by Table 1 and Table 2, variations in the feedback coefficient α and the pole radius ρ within their respective value ranges both affected the performance of the notch filter at a fixed notch frequency. Thus, the filter parameters were optimized using an intelligent optimization algorithm. In this study, the gray wolf optimization and genetic optimization methods were used. The genetic method was adopted because of its outstanding performance for multi-parameter optimization and fast convergence.

To minimize the sum parameter, objective functions based on direct summation, weighted summation, squared weighted summation, and normalized summation of the three parameters were constructed, and the optimization effects were

compared. Direct summation was applied. Genetic optimization is inspired by the biological evolutionary process. A computer is used to simulate the processes of replication, crossover, mutation, etc. and to select the optimal solution of the objective function in the solution space. The Non-dominated Sorting Genetic Algorithm (NSGA) is stratified according to the dominance relationship between individuals before the operator selection. The inputs of NSGA include the sum parameter, the notch frequency, and the value ranges for α and ρ. The outputs are the minimum value of the sum parameter and the optimal match of α and ρ. A flowchart of NSGA is shown in Figure 5.

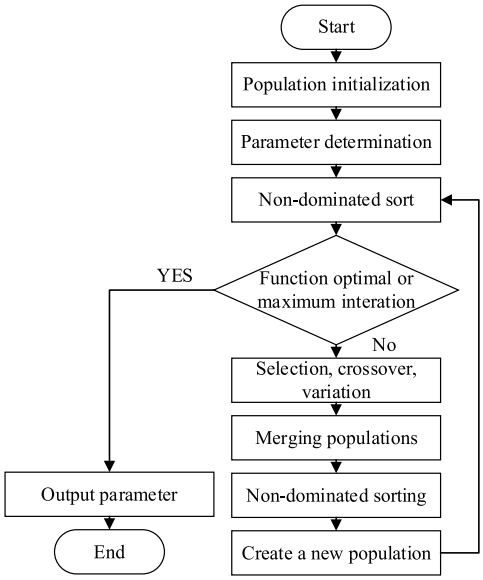

FIGURE 5. Flowchart of NSGA.

III. EXPERIMENTS AND RESULTS

An IR-UWB radar (X4M200, Novelda) and contact ECG signals (IX-B3G portable electrocardiograph) were used to validate the proposed method for real human vital-sign detection. Timestamps were used to synchronize the collected data. The radar had a center frequency of 7.29 GHz, a bandwidth of 1.4 GHz, and a pulse-repetition frequency (PRF) of 15.18 MHz. The sampling rate of the radar receiver is 23.328 GS/s and the frame rate in the slow-time is 17 FPS. The experimental setup is illustrated in Figure 6. The subject was lying down 0.5 m from the radar with normal breathing and was stationary.

The signal collection experiments were conducted on 10 adult subjects (five males and five females) aged between 21- and 45-years following protocol 2022-fhjsyxrc19 approved by Air Force Medical University, and all volunteers signed an informed consent form. Two sets of 20 normal breathing data with a duration of 45 s were collected, processed, and analyzed for each subject. A pair of RCG and ECG time-domain waveforms is shown in Figure 7. The black solid line represents the contact reference signal collected

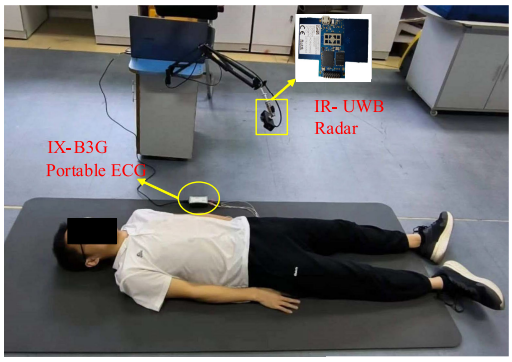

FIGURE 6. Experimental scenario for acquiring the respiratory signals and RCG.

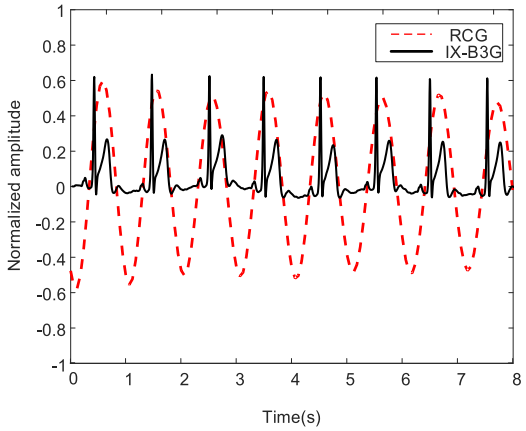

FIGURE 7. Pair of RCG and ECG time-domain waveforms.

from IX-B3G, and the red dashed line represents RCG. The absolute error percentage (AEP) [4] between the heart rates calculated from RCG and ECG was applied as an evaluation parameter. As shown in Figure 8, the AEPs for 10 pairs of RCG and ECG signals from 10 different volunteers were small, and the average AEP was 5.16%. The results indicated that the signals collected by the contact and contactless devices were highly consistent and that RCGs can be used for the detection of cardiac movement.

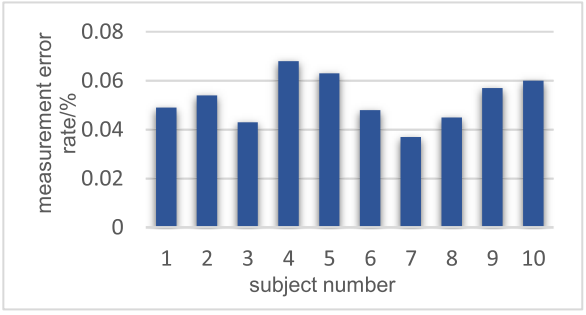

FIGURE 8. AEPs for 10 pairs of signals from 10 different subjects.

The respiratory signal and RCG spectra of one set of data before and after signal separation are shown in Figure 9.

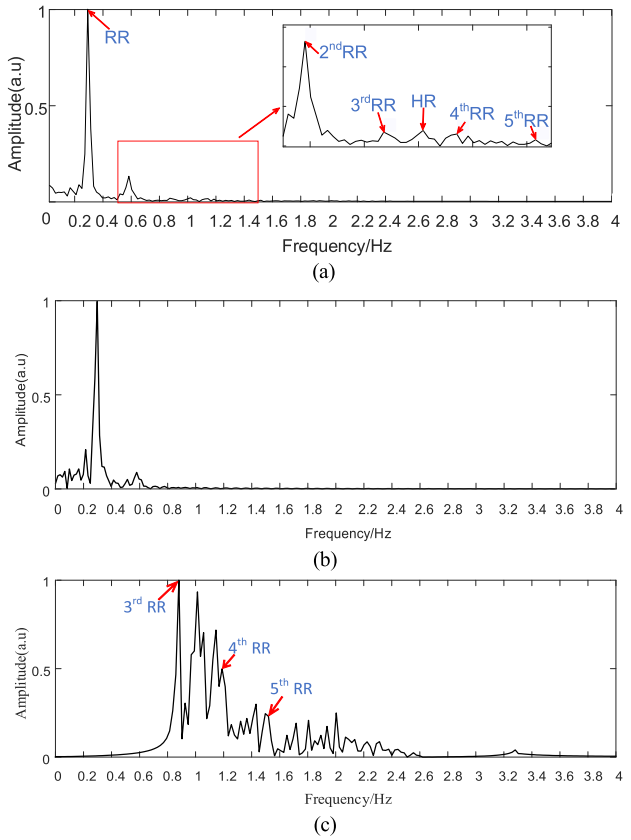

FIGURE 9. Frequency spectra of the respiratory signal and RCG before and after signal separation:(a) before signal separation (b) respiratory signal spectrogram; (c) RCG spectrogram.

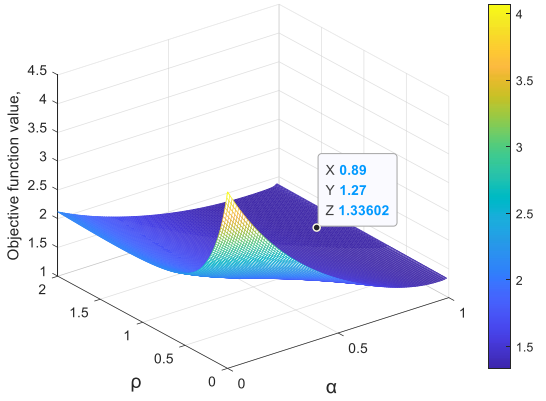

FIGURE 10. Parameters optimization results for a notch frequency of 0.897 Hz.

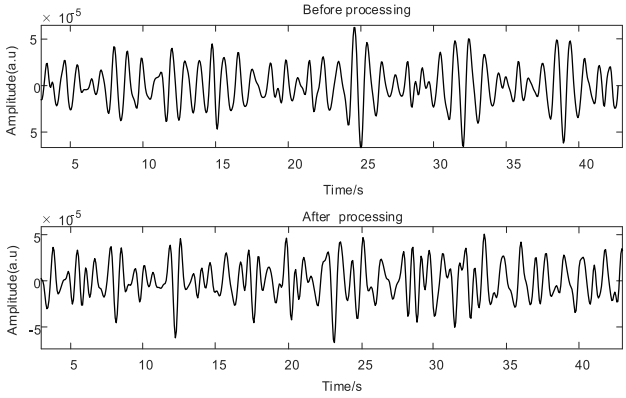

FIGURE 11. Time-domain waveforms before and after respiratory harmonic suppression.

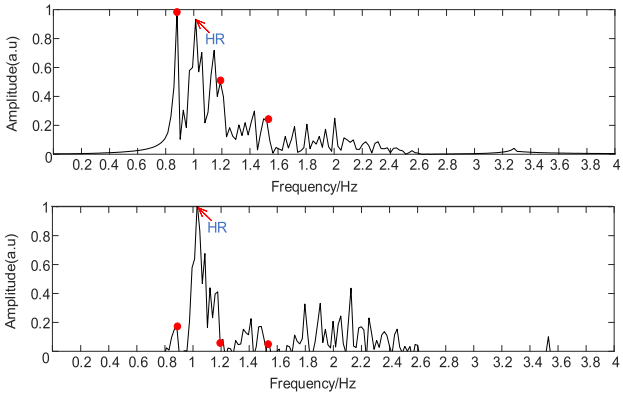

FIGURE 12. Spectrograms before and after respiratory harmonic suppression.

From Figure 9(a), it can be observed that the amplitudes of respiratory harmonics are high, with the second harmonic significantly higher than the amplitude of the heartbeat, while the third and fourth harmonics have amplitudes comparable to the heartbeat and cause interference. Since the respiration rate (RR) was approximately 18 beats per minute, corresponding to a fundamental frequency of respiration of 0.299 Hz, and the 2nd, 3rd, 4th, and 5th harmonics were 0.598, 0.897, 1.196, and 1.495 Hz, respectively. So, the second harmonic is outside the RCG band (0.8-2 Hz), and has been filtered during the separation step. Sequentially, each harmonic in the RCG was suppressed using a parameter-optimized feedback notch filter. The results of parameters (α and ρ) optimization for the 3rd harmonic frequency point of 0.897 Hz are shown in Figure 10. For the harmonic at this frequency point, when α and ρ were 1.27 and 0.89, respectively, the notch filter achieved the best performance. The time-domain and spectrogram results before and after the harmonic suppression are shown in Figures 11 and 12, respectively. The time-domain waveform in Figure 11 indicates that the respiratory envelope was reduced and the detailed information of the RCG was enhanced after the removal of the respiratory harmonics. Figures 12(a) and (b) present the spectrograms of the RCG before and after respiratory harmonic suppression, respectively. As shown, the heartbeat rate (HR) was approximately 60 beats per minute. After harmonic suppression, the frequency points of the three harmonics were significantly weakened with regard to amplitude.

The suppression results for the 20 datasets are presented in Table 3. The amplitude suppression ratio at each harmonic

TABLE 3. Suppression ratios of 3rd, 4th, and 5th respiratory harmonics.

Group	Third harmonic	Fourth harmonic	Fifth harmonic
1	83.6%	92.2%	93.5%
2	*	81.3%	75.9%
3	84.3%	88.5%	91.6%
4	*	92.3%	79.4%
5	81.3%	87.3%	85.3%
6	71.93%	90.85%	70.71%
7	78.62%	78.74%	83.78%
8	72.27%	85.85%	67.72%
9	84.44%	94.52%	92.76%
10	86.67%	53.60%	68.53%
11	90.74%	95.61%	83.70%
12	79.06%	62.90%	64.28%
13	95.73%	79.42%	61.47%
14	*	83.25%	68.74%
15	86.50%	50.16%	83.22%
16	61.38%	85.42%	71.17%
17	74.21%	73.51%	80.37%
18	52%	65.99%	87.02%
19	67.8%	69.60%	83.34%
20	90.72%	94.56%	82.97%

"∗" indicates that no third harmonic in the dataset fell within the RCG band.

frequency point was calculated using Equation (16).

$$AR = \frac{f_{ma} - f_{mb}}{f_{ma}} \times 100\% \tag{16}$$

Here, AR represents the amplitude suppression ratio, f_{ma} represents the amplitude of the harmonic frequency point before the suppression in the spectrogram, and f_{mb} represents the amplitude of the harmonic frequency point after the suppression.

The results in Table 3 indicate that the optimized feedback notch filter performed well, with average amplitude suppression ratios of 78.90%, 76.17%, and 79.81% for the third, fourth, and fifth harmonics, respectively. It was proven that the proposed method can effectively suppress respiratory harmonics while retaining the heartbeat component well, resulting in an optimized feedback notch filter.

IV. DISCUSSION

The RCG is a subtle signal with a small amplitude. Therefore, respiratory harmonics easily interfere with it, and they are difficult to suppress accurately using the existing methods. A novel feedback notch filter based on parameter optimization was proposed for the suppression of respiratory harmonic, taking into account the overlap between a certain respiratory harmonic and the corresponding cardiac sub-signal from the RCG. The effectiveness of the harmonic suppression method was verified through simulations as well as detection experiments involving humans. In particular, it can solve the problem of accurately separating signals with similar frequencies. This study is of considerable significance for noncontact RCG extraction and respiratory harmonic suppression. Additionally, it provides a technical basis for auxiliary diagnosis and monitoring using RCGs.

However, this study had limitations. In the experiment for detecting human vital signs, only the stationary state with a supine posture was considered. In future studies, we will consider more complex states of the human target, including random body movement, to make the proposed method more suitable for practical scenarios.

V. CONCLUSION

A respiratory harmonic suppression method employing correlation analysis and a genetically optimized feedback notch filter is proposed, which is based on 7.29 GHz center-frequency IR-UWB radar. The genetic optimization algorithm is applied to find the best match of parameters α and ρ; thus, the performance of the notch filter is optimized. According to the respiratory harmonic suppression results for 20 sets of data from 10 subjects, the average amplitude suppression ratio for all respiratory harmonics was 78.29%. The results verified that the proposed method can effectively locate, identify, and suppress respiratory harmonics from the RCG band while preserving heartbeat components well. Hence, it significantly increases the accuracy of RCG extraction. We envision that this method can be applied to various practical scenarios such as contactless auxiliary diagnosis and monitoring in intelligent medical and home healthcare.

ACKNOWLEDGMENT

The authors would like to thanks Dr. Fugui Qi for his valuable discussion and to Editage (www.editage.cn) for English language editing.

REFERENCES

[1] E. J. D. S. Luz, W. R. Schwartz, G. Càmara-Chàvez, and D. Menotti, "G-based heartbeat classification for arrhythmia detection: A survey," *Comput. Methods Programs Biomed.*, vol. 127, pp. 144–164, Apr. 2016, doi: 10.1016/j.cmpb.2015.12.008.

[2] Y. Zhang, F. Qi, H. Lv, F. Liang, and J. Wang, "Bioradar technology: Recent research and advancements," *IEEE Microw. Mag.*, vol. 20, no. 8, pp. 58–73, Aug. 2019, doi: 10.1109/MMM.2019.2915491.

[3] A. Mishra and C. Li, "A review: Recent progress in the design and development of nonlinear radars," *Remote Sens.*, vol. 13, no. 24, p. 4982, Dec. 2021, doi: 10.3390/rs13244982.

[4] D. Shi, F. Liang, J. Qiao, Y. Wang, Y. Zhu, H. Lv, X. Yu, T. Jiao, F. Liao, K. Yan, J. Wang, and Y. Zhang, "A novel non-contact detection and identification method for the post-disaster compression state of injured individuals using UWB bio-radar," *Bioengineering*, vol. 10, no. 8, p. 905, Jul. 2023, doi: 10.3390/bioengineering10080905.

[5] Y. Jing, F. Qi, F. Yang, Y. Cao, M. Zhu, Z. Li, T. Lei, J. Xia, J. Wang, and G. Lu, "Respiration detection of ground injured human target using UWB radar mounted on a hovering UAV," *Drones*, vol. 6, no. 9, p. 235, Sep. 2022, doi: 10.3390/drones6090235.

[6] A. Masiero, F. Fissore, and A. Vettore, "A low cost UWB based solution for direct georeferencing UAV photogrammetry," *Remote Sens.*, vol. 9, no. 5, p. 414, Apr. 2017, doi: 10.3390/rs9050414.

[7] P. Wang, Y. Zhang, Y. Ma, F. Liang, Q. An, H. Xue, X. Yu, H. Lv, and J. Wang, "Method for distinguishing humans and animals in vital signs monitoring using IR-UWB radar," *Int. J. Environ. Res. Public Health*, vol. 16, no. 22, p. 4462, Nov. 2019, doi: 10.3390/ijerph16224462.

[8] T. Zheng, Z. Chen, C. Cai, J. Luo, and X. Zhang, "V2iFi: In-vehicle vital sign monitoring via compact RF sensing," in *Proc. ACM Interact. Mob. Wearable Ubiquitous Technol.*, 2020, pp. 1–27.
[9] Y. Ma, F. Liang, P. Wang, H. Lv, X. Yu, Y. Zhang, and J. Wang, "An accurate method to distinguish between stationary human and dog targets under through-wall condition using UWB radar," *Remote Sens.*, vol. 11, no. 21, p. 2571, Nov. 2019, doi: 10.3390/rs11212571.
[10] F. Lin, C. Song, Y. Zhuang, W. Xu, C. Li, and K. Ren, "Cardiac scan: A non-contact and continuous heart-based user authentication system," in *Proc. 23rd Annu. Int. Conf. Mobile Comput. Netw.*, Oct. 2017, pp. 315–328.
[11] H. Shen, C. Xu, Y. Yang, L. Sun, Z. Cai, L. Bai, E. Clancy, and X. Huang, "Respiration and heartbeat rates measurement based on autocorrelation using IR-UWB radar," *IEEE Trans. Circuits Syst. II, Exp. Briefs*, vol. 65, no. 10, pp. 1470–1474, Oct. 2018, doi: 10.1109/TCSII.2018.2860015.
[12] Z. Duan and J. Liang, "Non-contact detection of vital signs using a UWB radar sensor," *IEEE Access*, vol. 7, pp. 36888–36895, 2019, doi: 10.1109/ACCESS.2018.2886825.
[13] Y. Wang, "Research on noncontact life sign information extraction technology based on ultra-broad-spectrum bioradar," Dept. Biomed. Eng., Air Force Med. Univ., Xi'an, China, Tech. Rep., 2009, doi: 10.7666/d.d219157.
[14] Y.-H. Lin, J.-H. Cheng, L.-C. Chang, W.-J. Lin, J.-H. Tsai, and T.-W. Huang, "A broadband MFCW agile radar concept for vital-sign detection under various thoracic movements," *IEEE Trans. Microw. Theory Techn.*, vol. 70, no. 8, pp. 4056–4070, Aug. 2022, doi: 10.1109/TMTT.2022.3186014.
[15] C. Zhu, M. Balle, B. Zhang, Q. Lv, Y. Li, Z. Zhu, X. Wang, X. Li, and L. Ran, "Doppler cardiogram detected by a V-band Doppler radar sensor," *IEEE Trans. Microw. Theory Techn.*, vol. 70, no. 1, pp. 521–531, Jan. 2022, doi: 10.1109/TMTT.2021.3128591.
[16] D. R. Morgan and M. G. Zierdt, "Novel signal processing techniques for Doppler radar cardiopulmonary sensing," *Signal Process.*, vol. 89, no. 1, pp. 45–66, Jan. 2009, doi: 10.1016/j.sigpro.2008.07.008.
[17] Y. Xiong, S. Chen, X. Dong, Z. Peng, and W. Zhang, "Accurate measurement in Doppler radar vital sign detection based on parameterized demodulation," *IEEE Trans. Microw. Theory Techn.*, vol. 65, no. 11, pp. 4483–4492, Nov. 2017, doi: 10.1109/TMTT.2017.2684138.
[18] S. Dong, Y. Li, J. Lu, Z. Zhang, C. Gu, and J. Mao, "Accurate detection of Doppler cardiograms with a parameterized respiratory filter technique using a K-band radar sensor," *IEEE Trans. Microw. Theory Techn.*, vol. 71, no. 1, pp. 71–82, Jan. 2023, doi: 10.1109/TMTT.2022.3184019.
[19] J.-H. Qiao, F.-G. Qi, F.-L. Liang, J. Ma, H. Lv, X. Yu, H.-J. Xue, Q. An, K.-D. Yan, D. Shi, Y.-H. Qiao, J.-Q. Wang, and Y. Zhang, "Contactless multiscale measurement of cardiac motion using biomedical radar sensor," *Frontiers Cardiovascular Med.*, vol. 9, pp. 1–13, Dec. 2022, doi: 10.3389/fcvm.2022.1057195.
[20] W. Liu, J. Liu, T. Liu, H. Chen, and Y.-L. Wang, "Detector design and performance analysis for target detection in subspace interference," *IEEE Signal Process. Lett.*, vol. 30, pp. 618–622, 2023.
[21] M. Alizadeh, G. Shaker, J. C. M. D. Almeida, P. P. Morita, and S. Safavi-Naeini, "Remote monitoring of human vital signs using mm-wave FMCW radar," *IEEE Access*, vol. 7, pp. 54958–54968, 2019, doi: 10.1109/ACCESS.2019.2912956.
[22] Y. Zhang, Y. Ma, X. Yu, P. Wang, H. Lv, F. Liang, Z. Li, and J. Wang, "A coarse-to-fine detection and localization method for multiple human subjects under through-wall condition using a new telescopic SIMO UWB radar," *Sens. Actuators A, Phys.*, vol. 332, Dec. 2021, Art. no. 113064, doi: 10.1016/j.sna.2021.113064.

YARU WANG received the B.E. degree from the Mingde College, Northwestern Polytechnical University, Xi'an, Shaanxi, China, in 2021. She is currently pursuing the M.E. degree with Xi'an Technological University, Xi'an.

She is also affiliated with the Bio-Radar and Signal Processing Laboratory, Department of Bio-Medical Engineering. Her research interest includes bioradar vital-sign detection.

JIAHAO QIAO received the B.E. degree in electronic information from Xi'an Technological University, Xi'an, China, in 2023. He is currently an Assistant Engineer with CLP Fenghua, Taiyuan, China. His research interests include bioradar noncontact vital signs detection and signal processing.

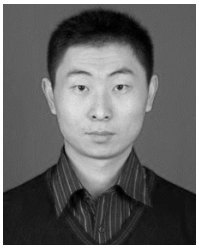

KEDING YAN received the B.E. degree from the North University of China, Taiyuan, Shanxi, in 2007, the M.S. degree from Xi'an Technological University, Xi'an, Shaanxi, in 2011, and the Ph.D. degree from Nanjing University of Science and Technology, in 2015. His research interests include inspection technology and automation and pattern recognition and intelligent systems.

DING SHI received the B.E. degree from Xi'an Traffic Engineering Institute, Xi'an, Shaanxi, China, in 2020, and the M.S. degree from Xi'an Technological University, Xi'an, in 2023. His research interests include radar non-contact detection and signal processing.

YIDAN ZHU received the B.E. degree from the Hi-Tech College, Xi'an University of Technology, Xi'an, Shaanxi, China, in 2021, where she is currently pursuing the M.E. degree.

She is currently affiliated with the Bio-Radar and Signal Processing Laboratory, Department of Bio-Medical Engineering. Her research interest includes EEG processing.

XINYU WANG received the B.E. degree from Xi'an Technological University, Xi'an, Shaanxi, China, in 2022, where she is currently pursuing the M.E. degree.

She is also affiliated with the Bio-Radar and Signal Processing Laboratory, Department of Bio-Medical Engineering. Her research interest includes bioradar vital-sign detection.

HUIJUN XUE received the B.E. and M.S. degrees from Shaanxi Normal University, in 2007 and 2010, respectively, and the Ph.D. degree in biophysics from Fourth Military Medical University (FMMU), Xi'an, Shaanxi, China, in 2018.

Since 2014, she has been a Lecturer with FMMU. Her research interests include detection and processing of noncontact biomedical signals.

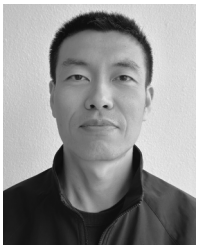

FULAI LIANG received the B.E., M.S., and Ph.D. degrees in information and communication engineering from the National University of Defense Technology, Changsha, Hunan, China, in 2006, 2008, and 2013, respectively.

He is currently an Associate Professor with Fourth Military Medical University. His research interests include modeling, signal processing, multiple human targets imaging, and detection and positioning.

XIAO YU received the B.E., M.S., and Ph.D. degrees from the Department of Bio-medical Engineering, Fourth Military Medical University (FMMU), Xi'an, Shaanxi, China, in 2003, 2006, and 2012, respectively. He is currently a Lecturer with FMMU. His research interests include distinguish between humans and animals based on bioradar and signal processing.

TENG JIAO received the M.S. degree in circuits and systems from the National University of Defense Technology, Changsha, Hunan, China, in 2002. His research interest includes detection and transmission of biomedical information.

HAO LV received the B.E., M.S., and Ph.D. degrees from Fourth Military Medical University (FMMU), Xi'an, Shaanxi, China, in 2004, 2007, and 2010, respectively. Since 2010, he has been teaching with the School of Biomedical Engineering, FMMU, where he has been an Associate Professor, since 2016. His research interests include biomedical signal processing and bioradar-based imaging.

JIANQI WANG was born in Xi'an, Shaanxi, China, in 1962. He received the B.E. degree from Xi'an Jiaotong University, Xi'an, in 1984, the M.E. degree from the National University of Defense Technology, Changsha, China, in 1990, and the Ph.D. degree from the Key Laboratory of the Ministry of Education of China, Xi'an Jiaotong University, in 2006. Since 1990, he has been teaching with the School of Biomedical Engineering, Fourth Military Medical University (FMMU), Xi'an, where he is currently a Professor and the Director of the Department of Medical Electronics, School of Biomedical Engineering. He pioneered radar-based human targets detection in China, in 1998, and has published more than 100 articles on related technologies. His research interests include bioradar-based signal processing, human target detection, imaging, and machine learning.

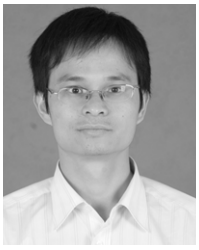

WENZONG LU received the B.E., M.S., and Ph.D. degrees from the College of Animal Science and Technology, Northwest A&F University, Yangling, Shaanxi, China, in 2002, 2006, and 2009, respectively.

His research interests include biomedical engineering, medical signal and image processing and analysis, mining, and analysis of biomedical data.

YANG ZHANG received the B.E., M.S., and Ph.D. degrees from the Department of Biomedical Engineering, Fourth Military Medical University, Xi'an, Shaanxi, China, in 2001, 2006, and 2009, respectively. He is currently an Associate Professor with the Bio-Radar and Signal Processing Laboratory, Fourth Military Medical University. From 2013 to 2014, he was a Visiting Scholar with the Department of Computer Science, Texas Tech University, Lubbock, TX, USA. His research interests include RF sensing, radar biomedical signal processing, target detection and positioning, and machine learning.